CONEM 2016
CONGRESSO NACIONAL DE ENGENHARIA MECÂNICA
21 - 25 AGOSTO DE 2016
FORTALEZA - CEARÁ

CORROSION BEHAVIOR OF LOW-TEMPERATURE PLASMA CARBURIZED AISI 420 STEEL - PART I - EFFECT OF TREATMENT TEMPERATURE

Cristiano José Scheuer, cristiano.scheuer@gmail.com[1,2]
Rodrigo Perito Cardoso, rodrigo.perito@ufpr.br[1]
Felipe Possoli, felipepossoli@gmail.com[3]
Paulo César Borges, pborges@utfpr.edu.br[3]
Silvio Francisco Brunatto, brunatto@ufpr.br[1]

[1] Plasma Assisted Manufacturing Technology & Powder Metallurgy Group, UFPR, 80531-980, Curitiba, PR, Brazil.
[2] Industrial Technical College, UFSM, 97105-900, Santa Maria, RS, Brazil.
[3] Academic Department of Mechanic, UTFPR, 80230-901, Curitiba, PR, Brazil.

Abstract: *The effect of plasma treatment parameters on the corrosion behavior of low-temperature carburized AISI 420 stainless steel was investigated by means of electrochemical measurements. The first part of this study (out of two), was conducted in order to evaluate the effect of the treatment temperature on the carburized samples corrosion resistance. Plasma carburizing treatments were performed at temperatures of 350, 400, 450 and 500 °C, for 8 and 12 h. The corrosion behavior was evaluated through open circuit potential and cyclic polarization test, using a solution of 3.0% NaCl as electrolyte. To support the discussions on corrosion behavior, XRD, microstructural analysis, and hardness measurements were also carried out. The results showed that low-temperature plasma carburizing treatment produced a carburized layer consisting of two parts, an outer layer (α'_C + Fe_3C) and a diffusion layer (α'_C). The electrochemical tests demonstrate that samples treated at temperatures between 350 and 450 °C exhibit higher corrosion potentials compared to untreated material, in the two studied treatment times. Moreover, the samples carburized at 500 °C showed lower corrosion potential compared to the untreated sample. Finally, an analysis of the corroded surface showed the predominance of pitting corrosion mechanism on samples treated at low temperatures (350-450 °C), intergranular corrosion for the samples treated at high temperature (500 °C), and widespread corrosion to the untreated sample.*

Palavras-chave: *low-temperature plasma carburizing, treatment parameters, martensitic stainless steel, expanded martensite, corrosion resistance, electrochemical tests.*

1. INTRODUCTION

Since the beginning of the last century, carburizing treatment proved to be an important surface treatment (Edenhofer *et al.* 2001). Thereafter, aiming to satisfy different industrial demands by a high controlled process, several plasma assisted techniques were developed (DC plasma (Corengia *et al.* 2004; Cheng *et al.* 2005; Leyland *et al.* 1993; El-Hossary *et al.* 2009), RF plasma (El-Hossary *et al.* 2001;Kim *et al.* 2003), plasma-based low-energy ion implantation (Lei and Zhu, 2005), and plasma immersion ion implantation (Mukherjee *et al.* 2002; Figueroa *et al.* 2005)). These techniques aiming to produce a surface layer with improved mechanical, wear and electrochemical properties (Scheuer *et al.* 2013). Depending on the treatment parameters, different behaviors forward the requests to which the treated material will be exposed. Thereat, a full understanding of the process parameters influence on process kinetics is mandatory. Among the parameters controlling carbon diffusion, temperature is one of the most important (Scheuer *et al.* 2013). Thereby, the correct choice of temperature will give the best combination between mechanical, tribological and electrochemical properties.

In this work a comprehensive study of the treatment temperature influence on microstructural characteristics and corrosion resistance of low temperature carburized AISI 420 martensitic stainless steel was performed.

2. EXPERIMENTAL PROCEDURE

2.1 Samples preparation

Cylindrical samples of 10 mm in height and 50.8 mm in diameter were cut from AISI 420 steel commercial rod (composition obtained by X-ray fluorescence: 0.31% C, 0.75% Mn, 0.36% Si, 13.68% Cr, 0.17%Ni, 0.04% P, 0.03% S,

0.06%Cu and Fe balance, in wt.%), supplied in the annealed condition, presenting a gross-equiaxed ferrite grain matrix and chromium carbide precipitates. To obtain a *bct* martensite structure, samples were air quenched from 1050 °C, after 0.5 h at the austenitizing temperature (the sample hardness in the as-quenched condition was 576±12 $HV_{0.3}$). After heat treatment, samples were ground using SiC sandpaper ranging from 100 to 1200 grade and polished using 1 μm Al_2O_3 abrasive suspension, in order to obtain a final mirror finish of a mean roughness Ra value around than 0.07 μm. Finally, samples were alcohol cleaned in ultrasonic bath and then introduced into the discharge chamber. Tempering and carburizing were simultaneously carried out. For comparison purpose, quenched samples were tempered in conventional furnace at 300 °C for 1 h, corresponding to reference sample (untreated) (the sample hardness after tempering was 489±10 $HV_{0.3}$).

2.2 Low-temperature plasma carburizing treatment

Carburizing treatments were carried out in a conventional plasma apparatus (composed by a 4.16 kHz square-wave pulsed dc power supply), which is illustrated and described in detail on Scheuer *et al.* (2013). Samples were placed on the cathode of this system, which was negatively biased at 700 V. The heating of the samples was a result of ions and fast neutral species bombardment. The mean power transferred to the plasma, and consequently the sample temperature, was adjusted by varying the switched-on time (t_{ON}) of the pulsed voltage. The temperature was measured by means of a chromel–alumel thermocouple (Ktype of 1.5 mm diameter) inserted 8 mm depth into the sample holder. Initially, the vacuum chamber was evacuated to a base pressure of 1.33 Pa with the help a dual-stage mechanical rotary pump. Prior to carburizing treatments, specimens were plasma sputter-cleaned in a gas mixture of 80% H_2+20% Ar, under a pressure of 400 Pa, at 300 °C for 0.5 h, aiming to remove the native surface oxide layer. Plasma carburizing was carried out using a gas mixture composition of 99.5% (80% H_2+20% Ar)+0.5% CH_4, in volume. The total gas flow rate and pressure were fixed at 1.67×10^{-6} $Nm^3\ s^{-1}$ and 400 Pa, respectively. Both the gas mixture composition and flow rate were fixed according to Scheuer *et al.* (2012), and the pressure and applied voltage in accordance with Scheuer *et al.* (2016). Samples were carburized at 350, 400, 450 and 500 °C, for constant times of 8 and 12 h. After carburizing, treated samples were cooled to room temperature under continuous flow of Ar and H_2 gas mixture (volume ratio: 1/4).

2.3 Surface and microstructural analysis

For microstructural analysis, samples were prepared by conventional metallographic procedure. After polishing, the cross-sectioned samples were etched using Marble's reagent (4 g of Cu_4SO_4 + 20 ml de HCl + 20 ml de H_2O). Samples were examined using an Optical Microscope (Olympus BX51M), and the thickness of the observed outer layers was determined by taking the mean of ten measurements using obtained images. The identification of the phases present in the treated layers was carried out by X-ray diffractometry (XRD), using a Shimadzu XRD 7000 X-ray diffractometer with a Cu Kα X-ray tube in the Bragg–Brentano configuration. The diffraction lines were taken with 2θ in the range of 30–60° with a scan speed of 0.1 θ/min. Surface roughness was measured using a Confocal Laser Scanning Microscope (Olympus LEXT OLS 3000). The measurements were made in a square area with 650 μm side, using a 20*x* objective lens, Gaussian filter and cut-off of 0.8 mm.

2.4 Electrochemical corrosion test

Electrochemical corrosion behavior of untreated and carburized AISI 420 steel samples were studied using potentiodynamic polarization technique. Cyclic potentiodynamic polarization curves were recorded according to the ASTM G61 standard, which is recommended for evaluating the pitting corrosion tendency of materials in chloride-containing media. The set up consisted of an Iviun Potentiostat/Galvanostat Model Iviun–n–Stat interfaced to a personal computer using the IviumSoft software, for data acquisition and analysis (using these software, the potentiodynamic polarization curves were plotted and both the corrosion current density (i_{cor}) and the zero current potential (E_{cor}) were estimated), and an electrochemical corrosion cell. Experiments were carried out at ambient temperature (25 °C ± 2) and open to the air, using a graphite rod as counter electrode (CE) and saturated calomel electrode (SCE) as a reference electrode, and the specimen (AISI 420 steel disc) as the working electrode. Prior to each experiment, the electrodes surface were degreased with acetone, rinsed with deionized water, and dried in flow of heated air. The electrolyte used was 3.5 wt. % NaCl (*pH* = 6.9), obtained from the high-purity NaCl (99%), mixed with distilled water. The specimen was clamped to the cell, sealing against a silicone gasket, which exposes 50.24 mm^2 of the specimen surface to the electrolyte. After stabilizing the open circuit potential (OCP) for 60 min, cyclic polarisation measurement was performed potentiodynamically at a scan rate of 1 mV s^{-1}, by setting a potential value of 100 mV below the OCP, in the positive direction until a threshold current density of 5.0 $mAcm^{-2}$ was reached. At this point, the potentiodynamic scan was reversed to the negative direction, and continued down to starting point. Each experiment was repeated at least three times to check the reproducibility and the scatter in the data are reported. The specimen area exposed to the corrosive solution was subsequently analyzed with optical microscopy, used the same microscope described above.

3. RESULTS AND DISCUSSION

3.1 Microstructural characterization

Cross section micrographs of the AISI 420 steel samples plasma carburized for 12 h at temperatures of 350, 400, 450 and 500 °C are shown in Figure 1 (a, b, c, d) respectively. A thin and continuous carbon-enriched layer (termed by Scheuer *et al.* (2012) as outer layer) is observed for all treatment studied conditions. According to XRD data presented on Figure 1, this layer is composed by a carbon supersaturated solid solution on martensite lattice (α'_C), and cementite iron carbide (Fe_3C), for samples treated at temperatures lower to 450 °C; and additionally chromium carbides (Cr_7C_3 and $Cr_{23}C_6$) for specimen carburized at 500 °C.

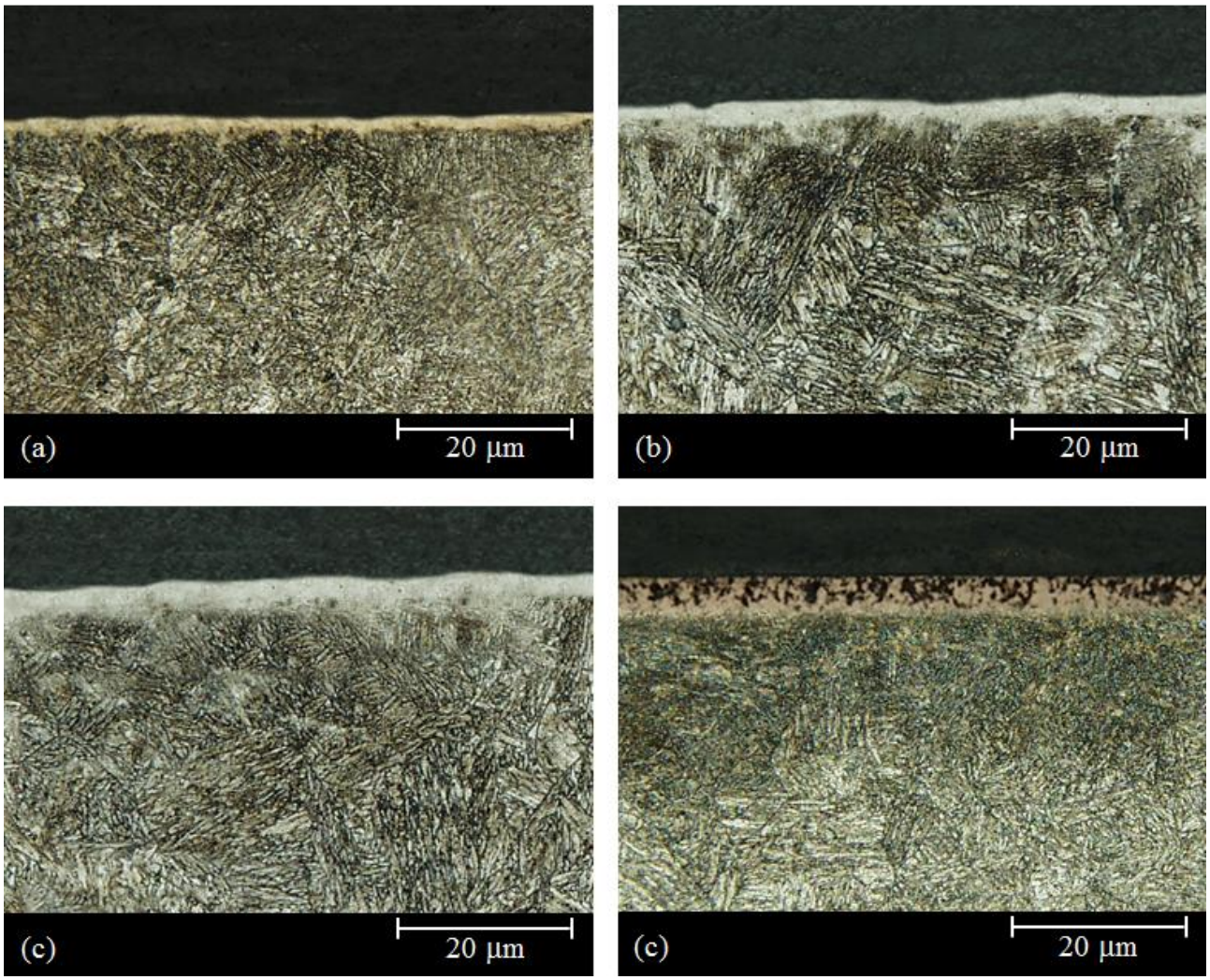

Figure 1. Cross-section micrographs of samples treated at: (a) 350; (b) 400; (c) 450; and (d) 500 °C

A study by Li *et al.* (2002), whose objective was to investigate the thermal stability of carbon expanded austenite (γ_C phase) formed in plasma carburized AISI 316 steel, indicated that γ_C decomposes in (Cr,Mo)C e $Cr_{23}C_6$ when annealed above a threshold temperature. It was demonstrated by Li *et al.* (2002) that for long-term treatment (20 h) this limit temperature was 400 °C. It was also found by Li *et al.* (2002) that γ_C phase is more thermally stable than the γ_N phase (nitrogen expanded austenite), since the last condition showed a thermal stability limit of 350 °C, for the same time of exposure. Therefore, given the observed sensitization to the 500 °C condition, it is supposed that the thermal stability limit of α'_C phase, stay between 450 to 500 °C for a 12 h exposure time. For AISI 420 steel plasma nitriding, Cardoso *et al.* (2016) demonstrated that for 4 h nitriding time, precipitation of chromium nitrides (CrN) occurs for treatment temperature of 450 °C, indicating that thermal stability of α'_N phase (nitrogen expanded austenite) is less than the α'_C phase.

Moreover, similar results those presented in Figure 1 were obtained on the treatments performed for 8 h at the same temperature range (which are present and discussed in previous paper Scheuer *et al.* (2013)), *id. est*, the occurrence of a thin and continuous carbon-enriched surface layer. In both treatments series, the outer layer thickness increasing with the carburizing temperature (Table 1). This result can be attributed to the increase in diffusivity of interstitial elements

with increasing treatment temperature Sun (2005). This behavior is expected for heat-activated treatments controlled by atomic diffusion. Activation energy for outer layer growth of 29 kJ mol^{-1} was obtained in both series of treatments. This value is consistent with that presented by Scheuer *et al.* (2013). Additionally, it is also verified the occurrence of a diffusion layer, which is evidenced by the more intensity etching of the region just below the outer layer, which is noticeable only in the micrograph of the sample carburized at 500 °C (Figure 1 d). Non-reported hardness profiles data indicate also the diffusion layer existence for the other conditions. The activation energy for the diffusion layer growth was 85 kJ mol^{-1}, agreeing with the results previously presented in Scheuer *et al.* (2013). The diffusion layer values are also presented in Table 1.

Table 1. Outer and diffusion layer thickness for samples carburized at 350, 400, 450 e 500 °C for 8 and 12 h.

Treatment condition	8 h		12 h	
	Outer layer	Diffusion layer	Outer layer	Diffusion layer
350 °C	1.5±0.1 μm	25 μm	1.8±0.1 μm	35 μm
400 °C	1.8±0.2 μm	40 μm	2.2±0.1 μm	50 μm
450 °C	2.2±0.2 μm	55 μm	2.6±0.2 μm	70 μm
500 °C	3.4±0.2 μm	65 μm	3.5±0.1 μm	75 μm

X-ray diffraction patterns of untreated (as-quenched) and plasma carburized samples treated at different temperatures for 12 h are shown in Figure 2. For the applied scan range (2θ from 30 to 60°), the as-quenched sample exhibit one peak reflection on the angle of 44.18°, which is attributed to the martensite phase (α′) (pdf-number 44-1290). XRD data of samples carburized at 350 to 450 °C for 12 h revealed the enlargement of the martensite peak, and its slight shift (~ 0.2°) for small 2θ angles. This result indicates the formation of the carbon-enriched martensite layer (α'_C phase). Furthermore, for those conditions, peaks relating to the iron carbide phase (Fe_3C) was also observed in the 2θ angles of 37.76, 39.78, 40.62, 43.73, 45,84 and 55.96° (pdf-numbers 03-1012, 34-0001, 72-1110, 76-1877, 77-0255, and 85-0871, respectively). The XRD pattern of the sample treated at 500 °C showed peak reflections related to Cr_7C_3 (2θ of 39.49 and 48.10 – pdf-number 11-0550) and $Cr_{23}C_6$ (2θ of 37.76, 48.10, 51.59, and 57.55° – pdf-numbers 03-1172, 03-1176 and 35-0783) chromium carbide phases. Finally, it is also observed that α'_C diffraction peak has disappeared giving place to α-Fe (110) (2θ of 44.28 – pdf-number 85-1410). This result indicates the α'_C phase decomposition as a consequence of the intense precipitation of chromium carbide phases for samples treated on this condition (500 °C). A similar behavior was observed by Scheuer *et al.* (2013) in treatments performed for 8 h at same temperature range.

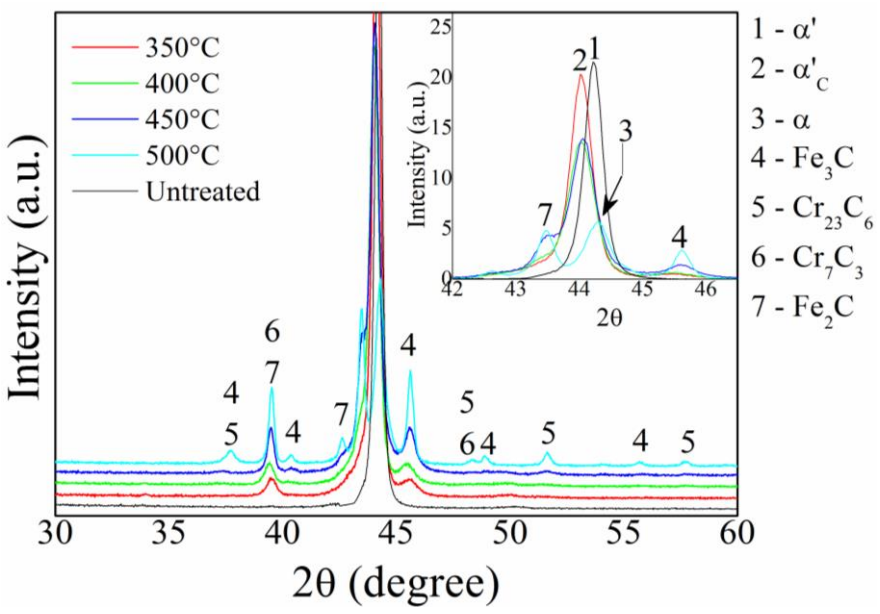

Figure 2. XRD patterns for untreated sample and for samples treated at 350, 400, 450 and 500 °C for 12 h.

3.2 Corrosion behavior

Results of open circuit potential test (OPC) for untreated and plasma carburized samples for 12 h at 350 to 500 °C are shown in Figure 3 (a) in terms of E_{OC} *vs.* time. Results show a rapid decrease of OCP values in the initial instants of the

sample immersion in corrosive solution, with subsequent stabilization. The trend of OCP decreasing values indicates the passive film dissolution on the electrolytic medium, showing the tendency of E_{OC} decreasing as a function of exposure time (Bernardelli *et al*. 2010). The posterior stabilization of OPC values indicates that a stable interface was produced between outer layer and the corrosive solution (Basso *et al.* 2010). The open circuit potential values are strongly dependent on the carburizing conditions (i.e., of the generated outer layer microstructure and chemical composition as a function of treatment time and temperature), as can be verified in Figure 3 (a) detail (OCP values were determined as the average of the last 20 min). The OCP of sample carburized at 400 °C stabilizes at a more positive (nobler) potential compared to the other conditions, indicating its likely greatest corrosion resistance in the studied environment. Confronting the OCP potential of untreated and 500 °C carburizing condition, it appears a decrease in the treated samples corrosion resistance compared the untreated condition, as a consequence of sensitization promoted by chromium carbide precipitation (previously showed in Figure 2). For other treatment conditions, the outer layer (precipitation free) possibly acts according the same passivation protection mechanism of passivating film, protecting the material core of aggressive external environment. With the increase of the outer layer thickness, increases the effectiveness of promoted protection, since greater is the time required for its dissolution, under the same corrosion rate. However, although the 450°C has shown a greater outer layer thickness, this condition showed stabilization in a more negative (less noble) potential, compared to 400 °C. According to the results presented above (Figure 1 e Figure 2), for this condition, the occurrence of sensitization and chromium carbide phase precipitation was not observed. It is assumed that although the microstructural characterizations did not show the occurrence of Cr carbides phases, it is possible that at this treatment temperature and time condition the chromium atoms have mobility through of the steel structure, and have achieved the stage of atoms clusters formation, which precede the carbides formation. This argument is confirmed by analysis of the E_{OC} *vs.* time behavior for sample carburized at 350 to 500 °C for 8 h (Figure 4 a). In this case, it appears that the OCP potential increases to a nobler values (more positive) with carburizing temperature in the range of 350 to 450 °C, which shows that for this treatment time the atoms mobility is limited to a level where there is no the formation of atoms clusters, which highlights the effect of carburizing time on the kinetics of atoms clusters formation. In contrast, for samples treated at 500 °C for 8 h, the OPC potential is less noble (more negative) compared to untreated samples, which is due to Cr precipitates formation for this condition, as presented in Scheuer *et al.* (2013). The comparison between the E_{OC} values for samples treated at 8 and 12 h (Table 2), shows that for the extreme treatment conditions (350 and 500 °C), the OPC values are approximately equal. For samples treated at 400 and 450 °C in turn, the open circuit potential values are quite different: for the first condition, the OCP values is nobler to 12 h samples, and for the second condition, the 8 h samples present a nobler OPC value. This result is related to the thickness, chemical composition and structure of the outer layer.

Figure 3 (b) present the cyclic polarization curves of the untreated and carburized samples treated for 12 h at temperatures between 350 to 500 °C (these curves were selected as being the most representative for each group of at least three tests carried out, providing a good approximation of the resulting average value). It can be verified a behavior similar to that presented in the OPC analysis: the corrosion potential (E_{cor}) becomes more negative for treating temperatures above and below 400 °C (Table 2), being this treatment condition which present the more noble corrosion potential. However, there is no passivation region for this condition as that demonstrated for the 350 and 450 °C. As known, the passivating region is indicated in a potentiodynamic curve through maintaining a current density approximately constant. The sharp increase of current density after continuous regime indicates the dissolution of the passivating film, with possible pits formation. The potential value for which occurs the sudden increase of the current density corresponds to the pitting potential (E_{PIT}). In some cases, according Wolynec (2003), even with the pitting mechanism occurrence, is not observed a sudden increase in current density, making it difficult or even impossible the determination of E_{PIT} value (which occurs for untreated and carburized 400 and 500 °C conditions). It is also verified by Figure 3 (b) analysis, that the potentiodynamic curves for untreated and 500 °C carburized samples are displaced upward, *i.e.* to higher current density values. This result also demonstrates the low corrosion resistance of these samples, indicating the occurrence of a higher corrosion rate (Basso *et al.* 2010; Wolynec, 2003) (confirmed by the calculated corrosion rate values presented in (Table 2). Furthermore, the positive hysteresis loop indicates the passive layer collapse with consequent pitting corrosion occurrence (Tait, 1994). According Tait (1994), the positive loop occur when the current density at the reversal scanning is larger than the in the positive scan direction, indicating the passive layer breaking (without recomposition) and pitting corrosion occurrence. Negative loop hysteresis, on the other hand, indicates that the passive film repairs itself alone, not allowing the initiation of pitting corrosion.

Figure 4 (b) shows the cyclic polarization curves of the untreated and plasma carburized specimens treated for 8 h at 350 to 500 °C. It was seen that the carburized samples did not have an evident passivation region, which indicates the progressive dissolution of treated layer, being confirmed by the positive loop hysteresis of potentiodynamic curve. Furthermore, with respect to corrosion potential it is noted the same behavior of the OCP values: E_{cor} increases to nobler values with increasing temperature in the 350 to 450 °C range, and reduction to a less noble potential compared to untreated condition with temperature increases to 500 °C (Table 2). Analogously to the OPC results, the comparison of the corrosion potential values of samples treated at 8 and 12 h shows that E_{cor} are similar for specimens treated at 350 and 500 °C, and different to samples treated at 400 and 450 °C maintaining the same E_{OC} pattern: for 400 °C, the E_{cor} is nobler to sample treated for 12 h while for 450 °C the 8 h treated samples present a nobler potential. These results are credited the different morphologies and dimensions of the outer layer depending on applied carburizing conditions.

Table 2. Electrochemical parameters obtained from the corrosion tests for samples treated at 8 and 12 h at 350, 400, 450 e 500 °C.

Treatment condition		Electrochemical parameters				
Time	Temperature	E_{OC} (V *x* NHE)	E_{COR} (V x NHE)	E_{PIT} (V x NHE)	i_{CORR} (mA/cm^2)	TC (mm/year)
8 h	350 °C	-0,13478	-0,1251	–	0,82	0,009
	400 °C	-0,06304	-0,0398	–	1,13	0,012
	400 °C	0,00845	0,0427	–	0,94	0,010
	500 °C	-0,18526	-0,2197	–	1,71	0,019
12 h	350 °C	-0,1445	-0,1291	0,3079	0,98	0,011
	400 °C	0,0442	0,0427	–	1,09	0,012
	400 °C	-0,0587	-0,0142	0,1634	1,12	0,012
	500 °C	-0,1819	-0,2395	–	1,53	0,017
Untreated (reference)		-0,1751	-0,1764	–	1,96	0,022

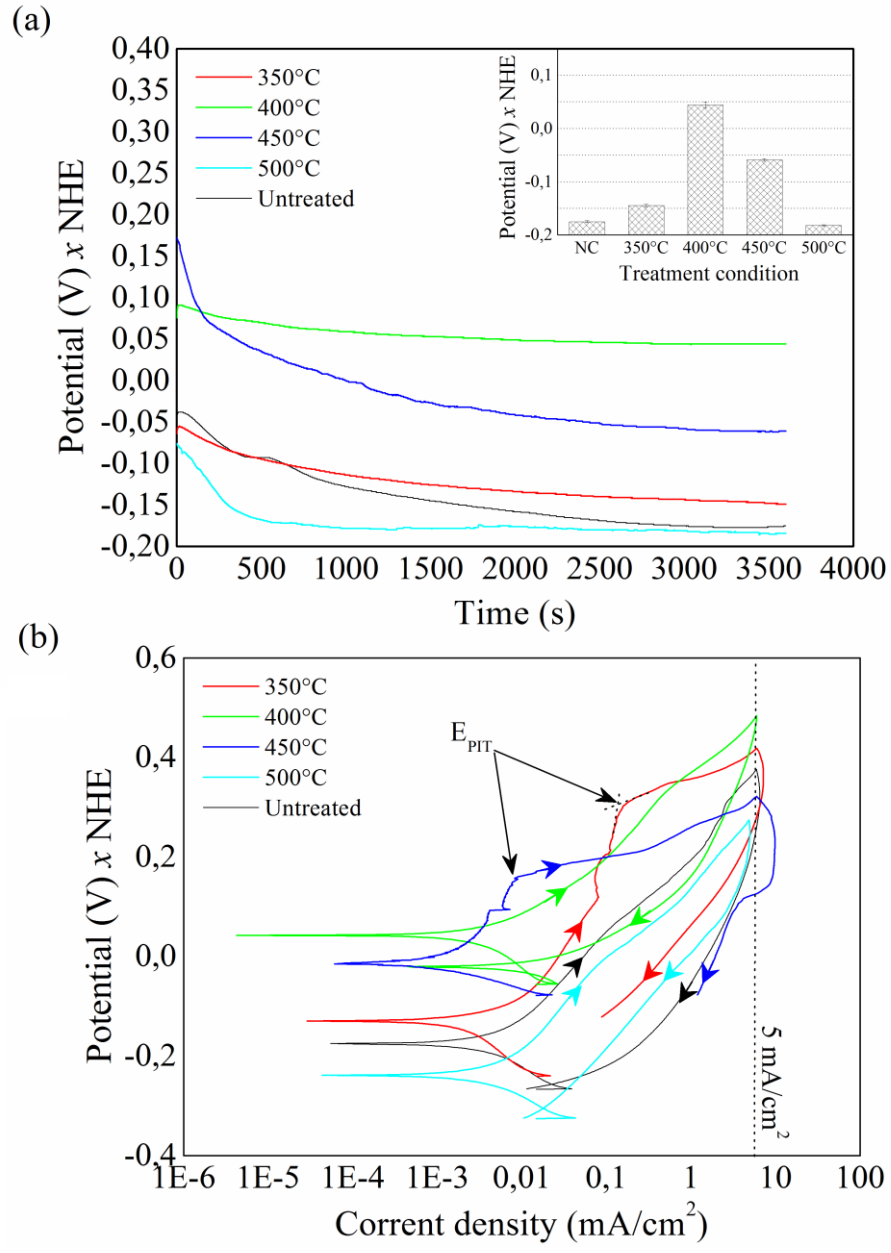

Figure 3. (a) Open circuit potential, and (b) potentiodynamic polarization curves achieved in a 3.5% NaCl solution of untreated and AISI 420 steel samples plasma carburized for 12 h at 350, 400, 450 and 500 °C.

The results presented in Figure 3 and Figure 4 confirm the effect of the different morphologies formed as a function of carburizing temperature and time on the carburized layer corrosion resistance. For the low-temperature treatment conditions (below 450 °C), the corrosion rate decreases as compared to the reference condition (Table 2), which is due to the outer layer formation (composed by α'_C e Fe_3C phases, as shown above). In fact, the formation of precipitation free interstitial solid solution supersaturated layers promotes an increase on stainless steels corrosion resistance. Regarding to nitrided martensitic stainless steels, several authors (Li and Bell 2006; Li and Bell 2007; Lu *et al.* 2016; Xi *et al.* 2008[a,b]) attribute the increase of corrosion resistance to composed layer formation (constituted by α'_N, ε-$Fe_{2-3}N$ e γ'-Fe_4N phases). In contrast, for carburized martensitic stainless steel, Li and Bell (2007) showed that the application of the treatment at 450 °C for 20 h does not promote a considerable increase in the corrosion resistance of the treated material when compared to untreated condition (as-quenched). As will be shown in the next paper (part II – study of the treatment time effect) for 450 °C treatment temperature, carburizing times longer than 12 h promote the reduction of martensitic stainless steel corrosion resistance, possibly due to atoms clusters formation. However, Heuer *et al.* (2010) showed that the application of gaseous carburizing treatment promotes a significant increase in PH13-8 Mo precipitation-hardened martensitic stainless steel corrosion resistance (in this case, the effect of steel composition on the diffusivity of interstitials elements should be considered, as demonstrated by (Tsujikawa *et al*. 2007; Tsujikawa *et al*. 2008; Ferreira *et* al. 2015) and on corrosion behavior (Pardo *et al.* 2008)). Furthermore, the increase of corrosion rate for samples carburized at 500 °C is assigned to chromium carbides precipitation occurrence and, consequently, Cr deflection. Similar result was also verified by the aforementioned authors (Li and Bell 2006; Li and Bell 2007; Lu *et al.* 2016; Xi *et al.* 2008[a,b]), in martensitic stainless steels nitrided at high temperatures (above 450 °C).

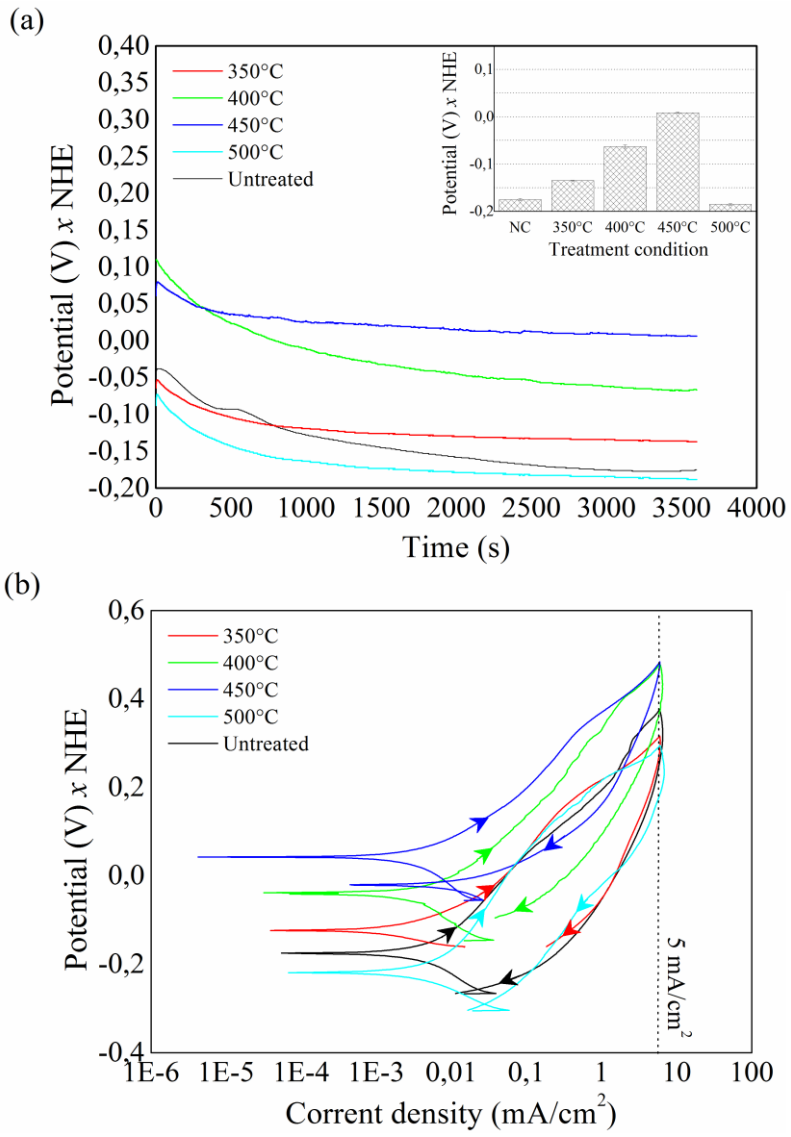

Figure 4. Open circuit potential, and (b) potentiodynamic polarization curves achieved in a 3.5% NaCl solution of untreated and AISI 420 steel samples plasma carburized for 8 h at 350, 400, 450 and 500 °C.

It is also possible to observe from Figure 3 and Figure 4, that for all the conditions discussed here the potentiodynamic curves does not show the occurrence of repassivation phenomenon (Cr_2O_3 passivation film formation). This result indicates that pits penetrate through the outer layer, and the passivating film did not regenerate over diffusion layer (Heuer *et al.* 2010). A possible explanation for this behavior is the reduction of the oxygen concentration inside the pit, preventing the repassivation. For the reference sample, the non-occurrence of repassivation phenomenon may be linked to the aggressiveness of corrosion medium, and it lower corrosion resistance in the tested corrosive environment. The aggressiveness of the corrosive medium prevents passivation, thus pitting corrosion continues propagating in an autocatalytic process, *i.e.*, the pitting corrosion process produces the conditions required for increasing the reaction rate.

Figure 5 (a-d) shows the surface morphology after electrochemical tests of the samples carburized at 12 h for 350, 400, 450 and 500 °C, respectively. It is possible to verify different behaviors in view of the employed treatment temperature. First, note that for 350 to 450 °C treatment conditions (Figure 5a-c), pitting corrosion mechanism is observed. The pits presence indicates that in some points the outer layer acts as the anode, while in the other regions it remain as the cathode (the noblest), which induces to localized corrosion (Bernardelli *et al*. 2010). The pits formation probably occurs due to defects in outer layer, to the presence of less noble and more anodic phases, and/or to the located depletion of chromium due to the formation of phases rich in this element. According Pardo *et al.* (2008) regions with highest density of crystalline defects (inclusions, dislocations, grain and phase boundaries), become more susceptible to pitting corrosion attack. It is also possible verify that the pits density is greater for the sample treated at 350 °C when compared to that carburized at 450 °C, confirming the superior corrosion resistance of the latter in the used corrosive environed, as shown previously on Figure 3. This is probably linked to the greater outer layer thickness of samples treated at 450 °C. Roberge (1999) showed that the corrosion resistance of chromium containing alloys is related to the layer thickness and homogeneity, and regions with faults or smaller thicknesses correspond to points of greater corrosion susceptibility. Likewise, the galvanic effect between the substrate and the treated layer is an additional factor for pitting formation and growth (Roberge, 1999). On the other hand, for sample carburized at 400 °C, a localized attack of small pits along the grain boundaries is verified (Figure 5b), supporting the argument exposed by Pardo *et al.* (2008) that regions with crystalline defects such as grain boundaries, are more susceptible to corrosion attack. One can also verify that the corroded area is smaller compared to other conditions, confirming its greater corrosion resistance, as indicated in the results of potentiodynamic tests and OCP. On the other hand, the sample carburized at 500 °C (Figure 5d) was severely damaged by corrosive attack. It is possible to note the occurrence of pits higher in size, and a more intense attack along the grain boundaries, confirming the lowest corrosion resistance for this condition previously indicated by the results presented in Figure 3. Finally, there was no occurrence of crevice corrosion.

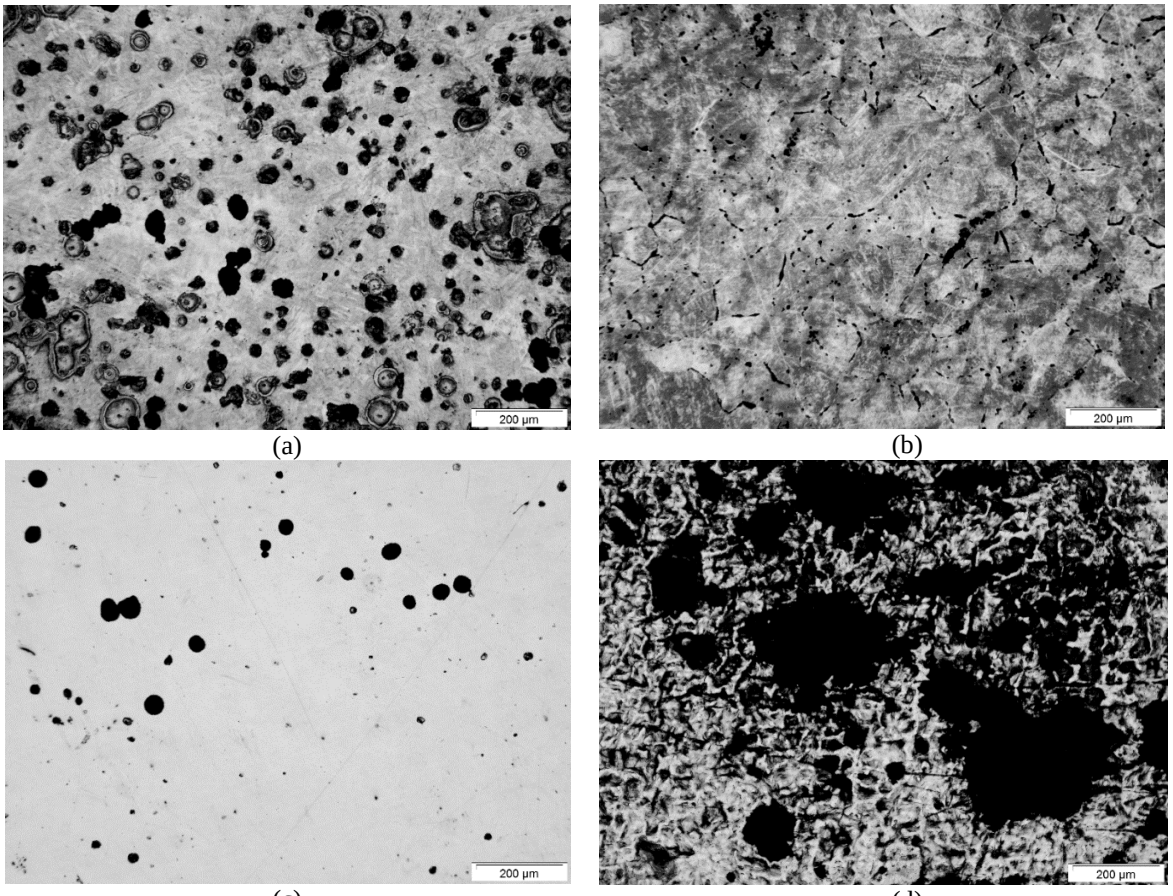

(a) (b)

(c) (d)

Figure 5. Optical microscopy morphologies of samples plasma carburized for 12 h at (a) 350, (b) 400, (c) 450 and (d) 500 °C after corrosive test.

The untreated samples (reference) also suffered a severely corrosive attack. As can be ascertained in Figure 6, the corrosive attack was uniform and generally along the surface exposed to corrosive solution. Pits are also verified. As mentioned above, the aggressiveness of the corrosive medium prevents repassivation, and pitting corrosion propagates in an autocatalytic process.

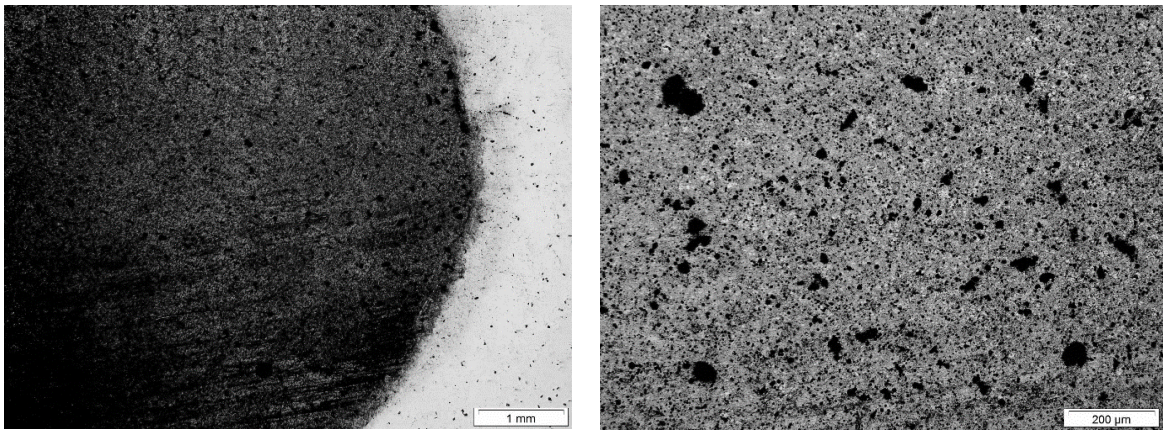

Figure 6. Optical microscopy morphology of reference sample (untreated) after corrosive test.

Figure 7 (a-d) shows the surface morphology after the potentiodynamic polarization test of samples plasma carburized for 8 h at 350–500 ºC, respectively. It is possible to verify the maintaining of same behavior seen in the results shown previously in Figure 5 for samples treated at 12 h: the occurrence of pitting corrosion mechanism for samples treated at low-temperatures (350 to 450 °C), and severely corrosive attack (higher size pits, and a intense attack along the grain boundaries) for sample treated at high temperature (500 °C). Specimens treated at 400 and 450 °C (Figure 7b and c) exhibit a less pronounced attack compared to those treated at 350 and 500 °C. These results corroborate those presented above on Figure 5(a-d). As discussed above, the higher corrosion resistance of samples treated at 400 and 450 °C when compared to that carburized at 350 °C, is related to greater outer layer thickness obtained for these conditions (Figure 7), agreeing with the argument presented by Roberge (1999). This also explains the fact that the sample treated for 12 h at this same temperature, presents an improved corrosion resistance when compared to treated 8 h. Moreover, the higher size pits and intense attack along the grain boundaries suffered by the sample carburized at 500 °C, is due to sensitization promoted by chromium carbide precipitation, as shown by Scheuer *et al.* (2013).

Ultimately, after each cyclic polarization test, the electrolyte was collected and analyzed as presence of solid precipitates, and measuring it *pH*. The remaining solutions of the tests performed on the samples carburized at 350 to 450 °C for 8 and 12 h showed no trace of solids precipitated, keeping a transparent coloration similar to exhibited in test beginning. In these cases, the electrolyte *pH* values after the tests remain similar to the starting. In contrast, the resulting electrolyte of the tests performed on the untreated and carburized at 500°C for 8 and 12 h samples, demonstrate an orange coloring, and a considerable amount of solid particles, indicating the formation of ferrous chloride ($FeCl_2$). The pH values determined from these electrolytes are lower than those measured at the beginning of the tests, which indicates an increase in the corrosive medium aggressiveness (Roberge, 1999).

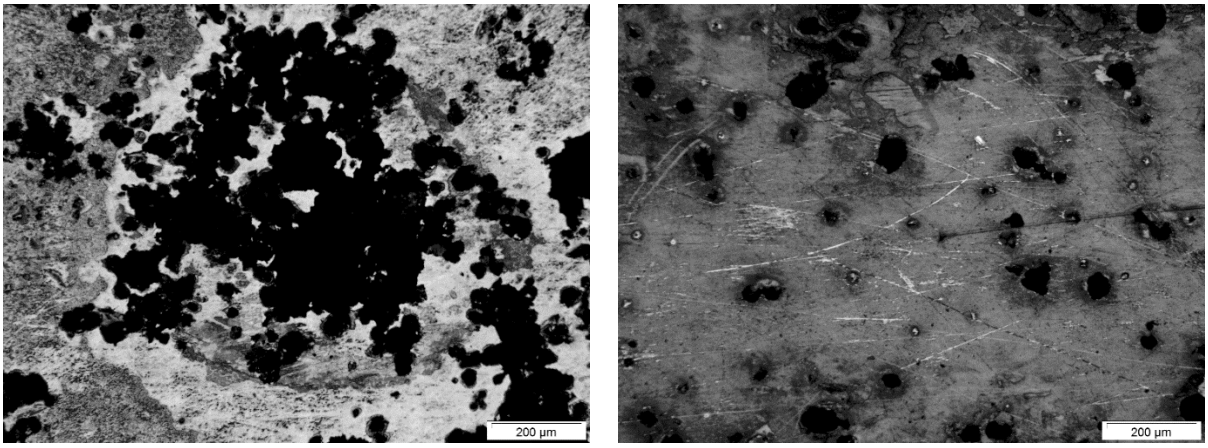

(a) (b)

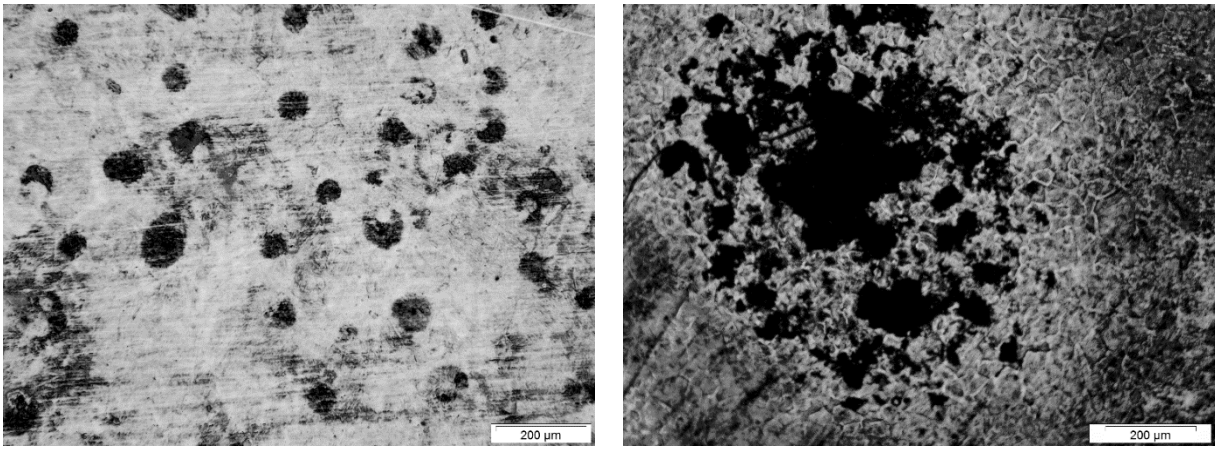

(c) (d)

Figure 7. Optical microscopy morphologies of samples plasma carburized for 8 h at (a) 350, (b) 400, (c) 450 and (d) 500 °C after corrosive test.

4. CONCLUSION

- Microstructural characterization revealed that carburized layer is formed through two distinct regions: an outer layer composed by Fe_3C and α'_C; and a diffusion layer, which is composed only by α'_C phase. It was also shown that the thickness of these two layers increases with increasing carburising temperature;
- Plasma carburized samples have a more noble corrosion behavior when compared to the reference sample (untreated), with the exception of those carburized at high temperature (500 ° C for 8 and 12 h). The improvement in the electrochemical behavior is due to the formation of a hardened layer ($Fe_3C + \alpha'_C$). The decrease in corrosion resistance for samples carburized at high temperature, is credited to the occurrence of chromium carbide phases precipitation, causing sensitization;
- The corrosion mechanism of carburized samples is the pitting corrosion. Samples carburized for 8 and 12 h at 500°C have been severely damaged by corrosive attack, being also verified the occurrence of grain boundaries corrosion mechanism. Reference samples suffered general corrosion throughout the entire length exposed to the corrosive solution.

5. REFERENCES

A.H. Heuer, A. Kahn, L.J. O'Donnell, F. Ernst, G.M. Michal, R.J. Rayne, F.J. Martin, P.M. Natishan. Electrochemical and Solid-State Letters 13 (2010) C37–C39.

A. Leyland, D.B. Lewisb, P.R. Stevenson, A. Matthews, Surf. Coat. Technol. 62 (1993) 608–617.

A. Pardo, M.C. Merino, A.E. Coy, F. Viejo, R. Arrabal, E. Matykina. Corrosion Science 50 (2008) 1796–1806.

ASTM G61: Standard Test Method for Conducting Cyclic Potentiodynamic Polarization Measurements for Localized Corrosion Susceptibility of Iron, Nickel or Cobalt-Based Alloys. USA, 2009.

B. Edenhofer, W. Gräfen, J. Müller-Ziller. Surf. Coat. Technol. 142 (2001) 225–234.

C.A. Figueroa, F. Alvarez, Z. Zhang, G.A. Collins, K.T. Short, J. Vac. Sci. Technol. A 23 (2005) 693–698.

C.J. Scheuer, R.P. Cardoso, M. Mafra, S.F. Brunatto. Surf. Coat. Technol. 214 (2013) 30–37.

C.J. Scheuer, R.P. Cardoso, F.I. Zanetti, T. Amaral, S.F. Brunatto. Surf. Coat. Technol 206 (2012) 5085–5090.

C.J. Scheuer, R.P. Cardoso, M. Mafra, S.F. Brunatto. *Submitted in Plasma Processes and Polymers.*

C.X. Li, T. Bell. Corrosion Science 48 (2006) 2036–2049.

C.X. Li, T. Bell. Materials Science and Technology 23 (2007) 355–361.

E.A. Bernardelli, P.C. Borges, L.C. Fontana J.B. Floriano. Kovové Materiály, 48 (2010) 105–116.

F.M. El-Hossary, N.Z. Negm, A.M. Abed El-Rahman, M. Hammad, Mater. Sci. Eng. C 29 (2009) 1167–1173.

F.M. El-Hossary, N.Z. Negm, S.M. Khalil, A.M. Abed El-Rahman, D.N. Mcilroy, Surf. Coat. Technol. 141 (2001) 194–201.

L.M. Ferreira, S.F. Brunatto, R.P. Cardoso.. Materials Research 18 (2015) 622-627.

M.K. Lei, X.M. Zhu. Surf. Coat. Technol. 193 (2005) 22–28.

M. Tsujikawa, M. Egawa, N. Ueda, A. Okamoto, T. Sone, K. Nakata. Surface and Coatings Technology 202 (2008) 5488-5492.

M. Tsujikawa, S. Noguchi, N. Yamauchi, N. Ueda, T. Sone. Surface and Coatings Technology 201 (2007) 5102-5107.

P. Corengia, G. Ybarra, C. Moina, A. Cabo, E. Broitman, Surf. Coat. Technol. 187 (2004) 63–69.

P.R. Roberge. Handbook of Corrosion Engineering. EUA: McGraw-Hill, 1999.

R.L.O. Basso, H.O. Pastore, V. Schmidt, I.J.R. Baumvol, S.A.C Abarca, F.S. DE Souza, A. Spinelli, C.A. Figueroa, C. Giacomelli, Corrosion Science 52 (2010) 3133–3139.

R.P. Cardoso, C.J. Scheuer, S.F. Brunatto. Encyclopedia of Iron, Steel, and Their Alloys. 1ed.: Taylor & Francis Group 2 (2016) 2153-2168.

S.K. Kim, J.S. Yoo, J.M. Priest, M.P. Fewell, Surf. Coat. Technol. 163–164 (2003) 380–385.

S. Mukherjee, P.M. Raole, P.I. John, Surf. Coat. Technol. 157 (2002) 111–117.

S. Wolynec. Técnicas Eletroquímicas em Corrosão. São Paulo: Editora da Universidade de São Saulo, 2003.

S.Y. Lu, K.F. Yao, Y.B. Chen, M.H. Wang, N. Chen, X.Y. Ge. Corrosion Science, *in press* (2015).

X.Y. Li, S. Thaiwatthana, H. Dong, T. Bell. Surface Engineering 18 (2002) 448–452.

W.S. Tait. An Introduction to Electrochemical Corrosion Testing for Practicing Engineers and Scientists. Pair O'Docs Publications, Racine, Wisconsin, 1994.

Y. Xi, D. Liu D.; D. Han. Surface and Coatings Technology 202 (2008) 2577–2583.

Y. Xi, D. Liu, D. Han. Applied Surface Science 254 (2008) 5953–5958.

Y. Sun. Journal of Materials Processing Technology. 168 (2005) 189–194.

Z. Cheng, C.X. Li, H. Dong, T. Bell. Surf. Coat. Technol. 191 (2005) 195–200.

Z. Cheng, C.X. Li, H. Dong, T. Bell, Surf. Coat. Technol. 191 (2005) 195–200.

6. RESPONSIBILITY NOTICE

The authors are the only responsibles for the content of this work.